



ELSEVIER

Composites: Part A 34 (2003) 183–193

**composites**

Part A: applied science  
and manufacturing

[www.elsevier.com/locate/compositesa](http://www.elsevier.com/locate/compositesa)

# A non-orthogonal constitutive model for characterizing woven composites

Pu Xue, Xiongqi Peng, Jian Cao\*

*Department of Mechanical Engineering, Northwestern University, 2145 Sheridan Road, Evanston, IL 60208, USA*

Received 7 November 2001; accepted 30 May 2002

## Abstract

Thermoforming of woven fabric reinforced composites usually results in significant in-plane shear deformation in materials, and induces additional anisotropy into the composite. In this paper, a new constitutive model for characterizing the non-orthogonal material behavior under large deformation is proposed. On the basis of stress and strain analysis in the orthogonal and non-orthogonal coordinates and the rigid body rotation matrices, the relationship between the stresses and strains in the global coordinates is obtained. The equivalent material properties are then determined by fitting the numerical load vs. displacement curves to experimental results under biaxial tension and pure shear conditions. This model can be used to efficiently predict material responses under various loading paths for woven composites with different weave architectures. The geometrical non-linearity and the material non-linearity, as well as the complex redistribution and reorientation of the warp and weft yarns during deformation are taken into account. To demonstrate the performance of this model, numerical simulations using a commercial finite element package (ABAQUS/Standard) incorporated with our material model are conducted for various loading cases. Numerical results are in excellent agreement with experimental data. © 2003 Elsevier Science Ltd. All rights reserved.

*Keywords:* A. Fabrics/textiles; B. Anisotropy; B. Mechanical properties; C. Finite element analysis (FEA)

## 1. Introduction

Made with high strength continuous fibers, structural composites are of increasing interest in automotive and aerospace industries due to their high strength/weight performance as compared to sheet metals. Nevertheless, significant reduction in manufacturing cost is required to use structural composites for mass production applications. Highly efficient thermo-stamping operations possess the potential to substantially reduce fabrication time and cost compared to the much slower autoclave forming process. To successfully investigate the formability of composite parts and optimize the processing parameters in thermo-stamping, an accurate and effective model of material behavior is essential.

Woven fabric reinforced composites have been recognized as more competitive than unidirectional composites in thermoforming due to their good stability and deformation characteristics resulted mainly from an area change due to the trellising of the yarns and secondly from the stretching of undulated fibers in the fiber directions. When the part geometry possesses a double curvature, the forming process usually results in significant in-plane shear deformation,

which consequently leads to complex redistribution and reorientation of fibers in the woven fabric reinforced composite. The change of fiber orientation during large deformation induces additional anisotropy into the composite. However, existing material models involving this non-orthogonality are very limited.

The pin-joint model, or so-called kinematic approach, was one kind of approach applied to simulate fabric forming [1–3]. In this model, the yarns were assumed to be pinned together at the crossover points of the weave, and the yarns were inextensible, incompressible, and free to rotate around the pin joints. The angle between the warp and weft yarns was used to measure the amount of shear deformation. Given the geometry of the formed shape and sufficient initial conditions of two perpendicular fiber directions in the formed configuration, the distribution and orientation of the rest of the fabric can be calculated. This method is fast and fairly efficient, and has established interfaces with CAD, which makes it easy to use. However, its solution generally relies on the initial path specified by users and does not account for the mechanical behavior of the fabric. The model was extended in Ref. [4] by introducing locally the influence of shear properties. By associating a shear angle with its corresponding shear energy, a unique final configuration can be obtained by minimizing the shear energy. The approach eliminates the ambiguity of

\* Corresponding author. Tel.: +1-847-467-1032; fax: +1-847-491-3915.  
E-mail address: [jcao@northwestern.edu](mailto:jcao@northwestern.edu) (J. Cao).

the traditional kinematic approach and preserves the advantage of being a fast solution solver. The effects of boundary conditions, such as friction and binder force, on fabric deformation and loads generated during the forming process, however, were not considered. The models mentioned above were only used to simulate the fabric forming.

For woven composites, there are two different approaches to predict the material properties and simulate the forming processes, i.e. in micromechanical and macroscopic approaches. The micromechanical approach is represented by the work of Hsiao and Kikuchi [5], which can take into account all geometrical and mechanical characteristics associated with the woven fabric and the resin, and is capable of calculating stresses in the microstructure. Nevertheless, it is time-consuming and computationally costly for complex fiber architectures and forming processes. The micromechanical approach for fabric can be found in Ref. [6], where the original fabric geometry, bending behavior, consolidation response, and flattening response are considered.

The macroscopic approach has its own merits because it is efficient and able to consider various bounding conditions and material behaviors provided that a good constitutive law is used. A lot of effort has been made in this area, such as the ‘mosaic model’ and the ‘fiber undulation model’ [7], which are orthogonal models, as well as the viscoelastic model [8], which considered the initial non-orthogonality of fibers, however, not its evolution. For flexible composites, four typical approaches taking into account the re-orientation of the fibers have been found in the literature. Luo and Chou [9, 10] presented two constitutive models based on the Eulerian description and the Lagrangian description, respectively. Their material was composed of continuous unidirectional fibers or sinusoidally shaped fibers in an elastomeric matrix, rather than woven fabric reinforced composite. Therefore, the composite lamina could be treated as a homogeneous 2D orthotropic elastic continuum, which is different from the woven composites. The nonlinear stress–strain relationship of the material, including the stretching–shear coupling, was obtained. The re-orientation of the unidirectional fiber was tracked by an iterative procedure. Blanlot and Billoët [11] proposed a mechanical approach, in which material behavior was assumed to be orthotropic in the frame that coincided with the directions of bisectors of the warp and weft roving, although the warp and weft directions were no longer orthogonal to each other after the shear deformation. The numerical formulation could characterize the evolution of the orthogonal hypoelastic law by updating the location of bisectors of the warp and weft roving. However, it is unclear how the material properties in the relative rotating frame were determined. Another model considering the non-orthogonal characteristics was presented by Vu-Khanh and Liu [12]. In the model thermo-mechanical properties of a deformed fabric composite (non-orthogonal architecture) were characterized by a laminate composed of four fictional, unidirectional plies  $[0_{h1}/90_{h2}/0_{h2}/90_{h1}]$ . On the basis of

classical laminated plate theory, the stiffness coefficients of the sub-ply model could be obtained and the thermal expansion properties of general woven fabric laminates with an arbitrary in-plane shearing deformation can be predicted. Although the effect of fiber undulation could be considered by experimentally measuring the equivalent thermal-elastic coefficients of the constituent plies, a refined model capable of directly incorporating the interaction of the plies into the model considering the architecture of the woven fabric is needed. Cherouat and Billoët [13] used a combination of truss elements and membrane elements to describe the deformation of woven composites during the shaping process. In the model, each warp and weft yarn was described by truss elements with elastic properties and the connecting points of truss elements were hinged, while the resin was modeled by membrane elements with viscous behavior. The latter was kinematically coupled to the fabric at those connecting points. This model can account for the specific deformation of the composite fabric and large angular variations of the yarns as well as the viscosity of the resin, but the model could not involve the bending stiffness of fabrics.

In order to accurately characterize the behavior of woven composites with different weave architectures in large deformation, a non-orthogonal constitutive model is proposed in this paper. We first summarize unique behaviors of woven composites in Section 2. Then, in Section 3, flexible shell elements are used to simulate the woven composite, which represent the fundamental large deformation mechanisms of weave architectures. The stress and strain relationship is established based on the stress and strain analysis in both the global orthogonal coordinates and the non-orthogonal material coordinates, together with the rigid body rotation matrices. The equivalent material properties of the shell element are determined by fitting the numerical force–displacement curves to the experimental data under biaxial tension and pure shear loadings. Finally, in Section 4, the predictions for biaxial tensions with different strain ratios and the trellising shear frame with composite misaligned, using a commercial finite element software (ABAQUS/Standard) incorporated with the proposed material model, are compared to the experimental results reported in Refs. [14,15]. To further understand this new model, the importance of the non-orthogonal transformation matrices and discussions on possible improvements are presented in Section 5.

## 2. Material characteristics

Generally, materials under the consideration of this new constitutive law are woven fabric reinforced composites under large deformation conditions. For materials to be used in thermo-stamping, it can be a commingled woven fabric with a thermoplastic matrix. The woven fabric consists of two sets of interlaced yarns. The lengthwise set is called *warp*, and the crosswise set is called *weft*. The yarns are composed of a large number of continuous fibers, while each

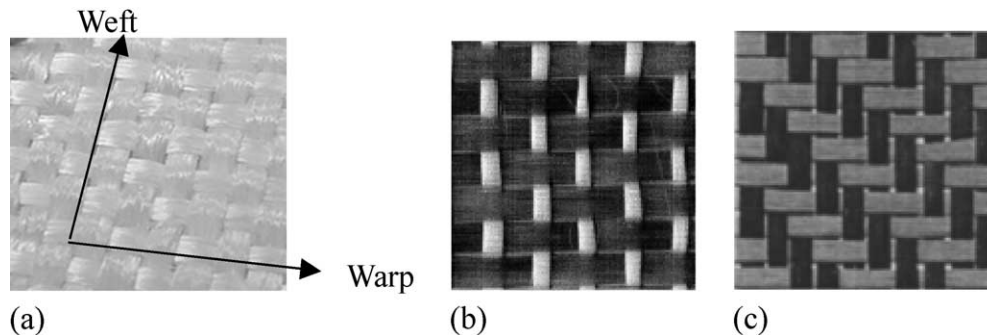


Fig. 1. Typical woven architectures: (a) balanced plain weave; (b) unbalanced plain weave [14]; (c)  $2 \times 2$  twill [14].

fiber has a typical diameter of  $5\text{--}20\ \mu\text{m}$  made of materials such as glass, carbon or aramid fibers. The high strength of these long, but slim fibers makes the fiber bundle have a high tensile stiffness along the yarn, however, a negligible compressive stiffness. A typical architecture of the woven fabric, balanced plain weave, is shown in Fig. 1(a), whose physical and geometrical properties can be considered as identical in the warp and weft directions. Fig. 1(b) and (c) shows the architectures of unbalanced plain weave and  $2 \times 2$  twill, respectively. All the architectures involve similar deformation mechanisms in nature and are summarized below:

- Forming woven fabric composites into complex shapes will lead to large shear deformation and the rearrangement of the fibers due to the trellising effect.
- The woven composite has a much smaller in-plane shear stiffness compared to tensile stiffness, and a negligible compressive stiffness during thermo-stamping.
- Undulation of yarns provides a soft response at the beginning of tension.
- Two initial superimposed yarns remain superimposed during the deformation process.

### 3. Constitutive model of woven fabric reinforced composites under large deformation

#### 3.1. Basic approach

The technology used in thermo-stamping of woven composites is similar to that for metal sheets, but deformation mechanisms involved during the deformation process are very different. In sheet metal forming, the blank is usually subjected to large membrane strains. However, in composite sheet forming, the fabric undergoes a small membrane extension while experiencing a large angular variation between the warp and weft yarns. An angle change greater than  $45^\circ$  is commonly observed. The specific deformation mechanisms, material discontinuity and the yarn interlacing make the woven fabric reinforced

composites behave quite differently from that of conventional continuum.

As mentioned before, the fiber size is typically around  $5\text{--}20\ \mu\text{m}$ , while the unit cell, which is the basic repeating pattern of the woven architecture, is in the order of centimeters, and finally the stamped part is in the order of meters. Due to various scales involved from micro to meso to macro, it would be too time-consuming to use continuum elements to reflect the architecture of a textile composite in simulating a stamping process, let alone optimizing. Therefore, flexible shell elements are used to simulate the woven composite and a constitutive law is needed to represent the fundamental deformation mechanisms of weave architectures under large deformation.

The establishment of the constitutive equation is based on the stress and strain analysis in the global orthogonal coordinates and the non-orthogonal material coordinates, together with the rigid body rotation matrices. The relationship between the stress and strain is updated at the end of each increment. The change of shell thickness is considered. The equivalent material properties of the shell element in material coordinates are determined by fitting the force–displacement curves obtained from our model to the experimental data under biaxial tension and pure shear loadings.

#### 3.2. Strain and stress analysis in the global orthogonal coordinates and the non-orthogonal material coordinates

It is assumed that the fabric under consideration has a symmetric plane that coincides with the middle surface of the fabric. In the following derivation, three sets of coordinates are selected on the middle surface. One is the global coordinate system with two orthogonal axes  $X$  and  $Y$  fixed in space. The second one is the local coordinate system with two orthogonal axes  $X'$  and  $Y'$ . The axis  $X'$  coincides with the current warp direction of the fabric. The third one is called the material coordinate system,  $O'\xi\eta$ , where  $\xi$  and  $\eta$  are chosen to coincide with the current warp and weft directions of the fabric, respectively. The axes  $\xi$  and  $\eta$  are orthogonal to each other at the original configuration, but

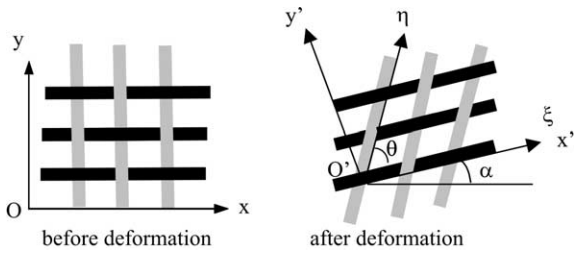


Fig. 2. Schematic of a deformed architecture with shear deformation. When  $\theta = 90^\circ$ , no shear deformation is involved.

will become non-orthogonal after shear deformation occurs, as shown in Fig. 2.

During the stamping operation, material points on the composite experience complex loading paths. Their deformation can be decomposed into two parts, i.e. the large shear deformation Fig. 2), and the tensile or compressive deformation. For the former one, a representative element is isolated, as shown in Fig. 3, by planes which are parallel to the axes  $\xi$  and  $\eta$ , respectively. Since  $O'\xi\eta$  is the non-orthogonal coordinate, the complementary property of shear stresses does not necessarily hold. Instead, two independent shear stress components,  $\tau_{\xi\eta}$  and  $\tau_{\eta\xi}$ , need to be introduced. Therefore, the stress state in the non-orthogonal coordinates  $O'\xi\eta$  can be expressed by four components, which are

$$[\sigma_\xi \quad \sigma_\eta \quad \tau_{\xi\eta} \quad \tau_{\eta\xi}]^T$$

The latter two components represent the shear stresses on the non-orthogonal planes, respectively. On the basis force equilibrium (Fig. 3), it can be obtained that

$$\begin{bmatrix} \sigma_{x'} \\ \sigma_{y'} \\ \tau_{x'y'} \end{bmatrix} = T_2 \begin{bmatrix} \sigma_\xi \\ \sigma_\eta \\ \tau_{\xi\eta} \\ \tau_{\eta\xi} \end{bmatrix} \quad (1)$$

where  $\sigma_{x'}$ ,  $\sigma_{y'}$ , and  $\tau_{x'y'}$  are stress components in the  $O'X'Y'$  coordinates, and  $\theta$  is the angle between the axes,  $\xi$  and  $\eta$ .  $T_2$  is a  $3 \times 4$  transformation matrix for the stress components from the non-orthogonal coordinates  $O'\xi\eta$  to the orthogonal coordinates  $O'X'Y'$  and can be expressed as

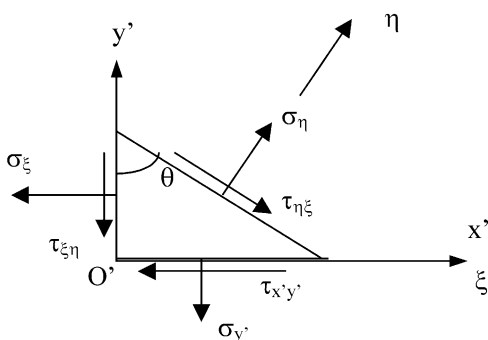


Fig. 3. An isolated element and its stress components.

$$T_2 = \begin{bmatrix} 1 & 0 & 0 & 0 \\ 0 & 1 & -\cot \theta & -\cot \theta \\ -\cot \theta & \cot \theta & 0 & 1 \end{bmatrix} \quad (2)$$

Correspondingly, it is also necessary to introduce four strain components in the local non-orthogonal coordinates, which are

$$[\varepsilon_\xi \quad \varepsilon_\eta \quad \gamma_{\xi\eta} \quad \gamma_{\eta\xi}]^T$$

where  $\varepsilon_\xi$  and  $\varepsilon_\eta$  are the normal strains along the warp and weft directions, respectively, and  $\gamma_{\xi\eta}$  and  $\gamma_{\eta\xi}$  are the shear strains reflecting the angular change from a right angle formed by axes  $\xi$  and  $\eta$  at the initial position. Based on the strain analysis, we have

$$\begin{bmatrix} \varepsilon_\xi \\ \varepsilon_\eta \\ \gamma_{\xi\eta} \\ \gamma_{\eta\xi} \end{bmatrix} = T_3 \begin{bmatrix} \varepsilon_{x'} \\ \varepsilon_{y'} \\ \gamma_{x'y'} \end{bmatrix} \quad (3)$$

where  $T_3$  is a  $4 \times 3$  transformation matrix connecting the strain components between the non-orthogonal coordinates  $O'\xi\eta$  and the orthogonal coordinates  $O'X'Y'$ , and it can be shown as

$$T_3 = \begin{bmatrix} 1 & 0 & 0 \\ \cos^2 \theta & \sin^2 \theta & \sin \theta \cos \theta \\ 0 & 0 & 1 \\ 0 & 0 & 1 \end{bmatrix} \quad (4)$$

It has been verified experimentally in the biaxial tensile test by Boisse's group [14,16] that the shear stresses/strains and the normal stresses/strains can be treated as uncoupled in the material coordinates  $O'\xi\eta$ . Fig. 4(a) shows the experiment set-up and Fig. 4(b) shows that the angle between weaving directions has a negligible influence on the biaxial tensile behavior. Therefore, the relationship between stress and strain components for woven composites can be approximately expressed as

$$\begin{bmatrix} \sigma_\xi \\ \sigma_\eta \\ \tau_{\xi\eta} \\ \tau_{\eta\xi} \end{bmatrix} = \begin{bmatrix} D_{11} & D_{12} & 0 & 0 \\ D_{21} & D_{22} & 0 & 0 \\ 0 & 0 & \beta D_{33} & 0 \\ 0 & 0 & 0 & (2 - \beta)D_{33} \end{bmatrix} \begin{bmatrix} \varepsilon_\xi \\ \varepsilon_\eta \\ \gamma_{\xi\eta} \\ \gamma_{\eta\xi} \end{bmatrix} = D \begin{bmatrix} \varepsilon_\xi \\ \varepsilon_\eta \\ \gamma_{\xi\eta} \\ \gamma_{\eta\xi} \end{bmatrix} \quad (5)$$

where  $\beta$  is a coefficient which stands for the contribution to the total shear property from each shear stress.  $D$  is

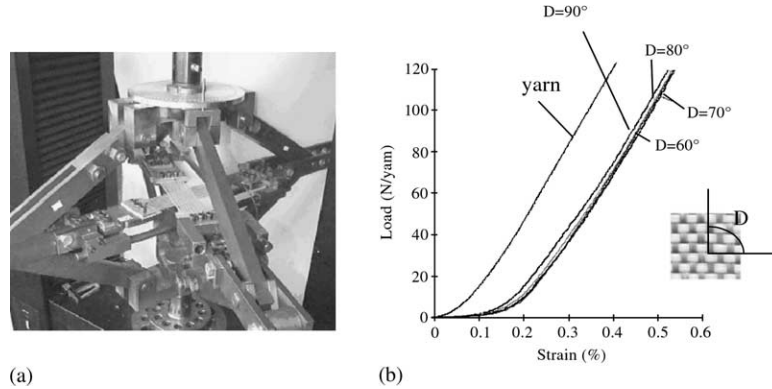


Fig. 4. Biaxial tensile test in the non-perpendicular configuration [14]. (a) Biaxial tensile device; (b) effect of the angle between yarn tows on the balanced plain weave fabric behavior.

a material matrix in the coordinate system  $O'\xi\eta$ ;  $D_{11}$ ,  $D_{12}$ ,  $D_{21}$  and  $D_{22}$ , which describe the tensile properties of the woven composite, are non-linear functions of the effective strain defined in Eq. (19). For the balanced woven fabric,  $D_{11} = D_{22}$ ,  $D_{12} = D_{21}$  and  $\beta = 1$ . The element  $D_{33}$  in Eq. (5) denotes the shear property of the material and can be assumed as a function of the shear strain only. In Eq. (5),  $\tau_{\xi\eta}$  and  $\tau_{\eta\xi}$  are not independent, and should satisfy the equation

$$\tau_{\xi\eta} + \tau_{\eta\xi} = \beta D_{33} \gamma_{\xi\eta} + (2 - \beta) D_{33} \gamma_{\eta\xi} = 2D_{33} \gamma_{\xi\eta} \quad (6)$$

Combining Eqs. (1)–(5), the relationship between the stress and strain components in the coordinate system  $O'X'Y'$  can be expressed as

$$[\sigma]_{X'Y'} = \bar{D}[\varepsilon]_{X'Y'} \quad (7)$$

where

$$\bar{D} = T_2 D T_3 \quad (8)$$

$\bar{D}$  is the material matrix in the coordinate system  $O'X'Y'$ , which varies with the strain status.

Then, the constitutive equation of woven composite in global coordinate system  $OXY$  under large deformation can be expressed as

$$\begin{bmatrix} \sigma_x \\ \sigma_y \\ \tau_{xy} \end{bmatrix} = R \bar{D} R^T \begin{bmatrix} \varepsilon_x \\ \varepsilon_y \\ \gamma_{xy} \end{bmatrix} = R T_2 D T_3 R^T \begin{bmatrix} \varepsilon_x \\ \varepsilon_y \\ \gamma_{xy} \end{bmatrix} \quad (9)$$

where  $R$  is the unit transformation matrix between the local orthogonal coordinates  $O'X'Y'$  and the global orthogonal coordinates  $OXY$  [17].  $R$  can be expressed in terms of  $\alpha$  in Fig. 2 as

$$R = \begin{bmatrix} \cos^2 \alpha & \sin^2 \alpha & -2 \sin \alpha \cos \alpha \\ \sin^2 \alpha & \cos^2 \alpha & 2 \sin \alpha \cos \alpha \\ \sin \alpha \cos \alpha & -\sin \alpha \cos \alpha & \cos^2 \alpha - \sin^2 \alpha \end{bmatrix} \quad (10)$$

If the material mainly experiences tensile or compressive deformation, the transformation matrices  $T_2$  and  $T_3$  become

$$T_2 = \begin{bmatrix} 1 & 0 & 0 & 0 \\ 0 & 1 & 0 & 0 \\ 0 & 0 & 0 & 1 \end{bmatrix} \quad (11)$$

and

$$T_3 = \begin{bmatrix} 1 & 0 & 0 \\ 0 & 1 & 0 \\ 0 & 0 & 1 \\ 0 & 0 & 1 \end{bmatrix} \quad (12)$$

Then, the material matrix in the orthogonal coordinate system is

$$\bar{D} = T_2 \times D \times T_3 = \begin{bmatrix} D_{11} & D_{12} & 0 \\ D_{21} & D_{11} & 0 \\ 0 & 0 & (2 - \beta) D_{33} \end{bmatrix} \quad (13)$$

Therefore, the relationship between the stress and strain components can be expressed as

$$\begin{bmatrix} \sigma_{x'} \\ \sigma_{y'} \\ \tau_{x'y'} \end{bmatrix} = \begin{bmatrix} D_{11} & D_{12} & 0 \\ D_{21} & D_{22} & 0 \\ 0 & 0 & (2 - \beta) D_{33} \end{bmatrix} \begin{bmatrix} \varepsilon_x \\ \varepsilon_y \\ \gamma_{xy} \end{bmatrix} \quad (14)$$

The constitutive equation (Eq. (7)) in this case reduced to the general expression for an orthogonal material.

### 3.3. New effective strain definition

Considering the characteristics of flexible woven composites, it is necessary to define a new effective strain in this case. In general, the equivalent strain is defined as [18]

$$\bar{\varepsilon} = \sqrt{\frac{2}{9} [(\varepsilon_1 - \varepsilon_2)^2 + (\varepsilon_2 - \varepsilon_3)^2 + (\varepsilon_3 - \varepsilon_1)^2]} \quad (15)$$

where  $\varepsilon_1$ ,  $\varepsilon_2$  and  $\varepsilon_3$  are three principal strains.

In the case of thin sheets, the incompressibility of material leads to

$$\varepsilon_1 + \varepsilon_2 + \varepsilon_3 = 0 \tag{16}$$

Thus, Eq. (15) can be rewritten as

$$\begin{aligned} \bar{\varepsilon} &= \sqrt{\frac{2}{9}[(\varepsilon_1 - \varepsilon_2)^2 + (2\varepsilon_2 + \varepsilon_1)^2 + (2\varepsilon_1 + \varepsilon_2)^2]} \\ &= \frac{2}{\sqrt{3}}\sqrt{\varepsilon_1^2 + \varepsilon_2^2 + \varepsilon_1\varepsilon_2} \end{aligned} \tag{17}$$

Since flexible woven composites cannot effectively sustain compressive load, the negative strain(s) would not contribute to the load-carrying capability of the material. In this case, the effective normal strains along each of the fibers' directions can be defined as

$$\varepsilon_i^+ \equiv \frac{\varepsilon_i + |\varepsilon_i|}{2} = \begin{cases} \varepsilon_i & \varepsilon_i > 0 \\ 0 & \varepsilon_i \leq 0 \end{cases} \quad i = 1, 2 \tag{18}$$

Then, the effective strain can be defined as

$$\bar{\varepsilon}^+ = \frac{2}{\sqrt{3}}\sqrt{(\varepsilon_1^+)^2 + (\varepsilon_2^+)^2 + (\varepsilon_1^+)(\varepsilon_2^+)} \tag{19}$$

It should be noted that for some woven fabrics, such as balanced plain weave or 2 × 2 twill weave with high density, there are less voids in the material. The constitutive model developed here can be applied well to predict the material properties and various responses. For materials with more voids, the assumption of incompressibility will not hold, however, the non-orthogonal framework still sustains. To specifically address the void effect, the relationship between the strains needs to be modified, and this will be a part of our future work. In the validation cases presented in Section 4, the predictions and the experimental results agree well for woven fabric with different architectures even with the incompressibility assumption. The reason for this success is that the equivalent material properties are obtained by fitting the predictions to the experimental data that already involved the voids effect in.

### 3.4. Determination of the equivalent material properties

The material matrix, *D*, can be determined by matching the force–displacement curves calculated from our model with the experimental data under uniaxial tension or biaxial tension and pure shear loadings. For a balanced woven fabric, only the elements, *D*<sub>11</sub>, *D*<sub>12</sub> and *D*<sub>33</sub>, need to be determined.

Due to the limitation of the experimental data available to us, the data from each material configuration [14,19] are not enough to determine all the properties in the material matrix, *D*. There is an on-going effort to perform benchmarks on material testing and thermo-forming of textile composites [20], and the results are expected in two years. Here, we have to use testing data of two different materials

to demonstrate our approach. The experimental data used to determine the tensile properties are from Buet-Gautier and Boisse's [14] for a balanced plain weave glass fabric, and those used to obtain the shear property are from Chen and Lussier [19] for a woven composite with balanced plain weave reinforcement, which comprised commingled glass and polypropylene (PP) yarns with a glass volume fraction of 0.7.

#### 3.4.1. Determination of the tensile properties

Buet-Gautier and Boisse [14] reported their experimental results for the balanced plain weave glass fabric in uniaxial tension and biaxial tensile tests at several strain ratios *k* =  $\varepsilon_{\text{weft}}/\varepsilon_{\text{warp}}$ . The fabric density (yarn/mm) was 0.22, which is defined by the number of yarns per unit length. The crimp characterizing undulation of the fabric was 0.4%. Fig. 5 shows the geometry and material behaviors under unequal biaxial tension conditions at the strain ratio *k* =  $\varepsilon_{\text{weft}}/\varepsilon_{\text{warp}}$  = 2.

In order to determine the tensile properties of the material, a composite patch with the same fabric geometry as the tested sample is considered. Unequal biaxial extensions are imposed at the corresponding strain ratio used in the test. The composite patch is simulated using shell elements (ABAQUS type S4R) in finite element software (ABAQUS/Standard) incorporated with our material model as a user material subroutine. By fitting the simulated load vs. displacement curve to the experiment

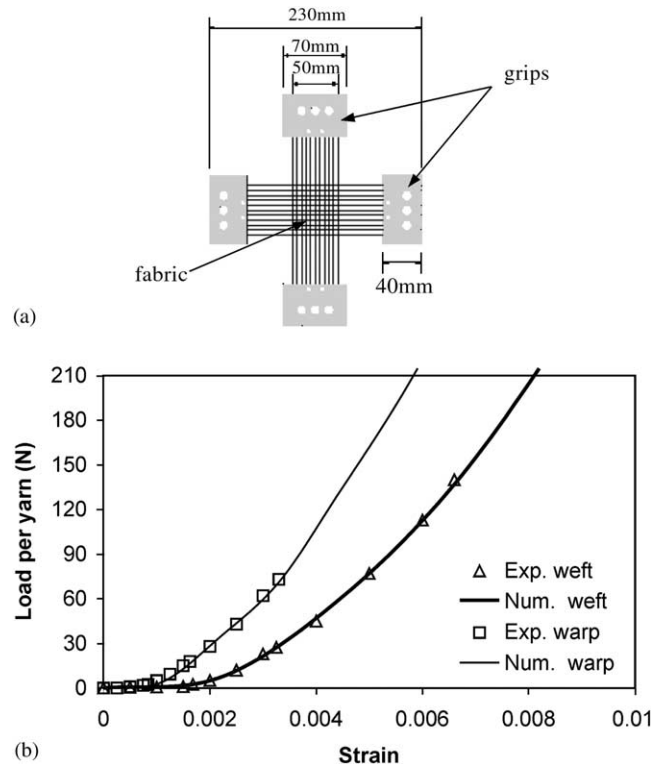


Fig. 5. Unequal biaxial tension. (a) Sample geometry; (b) load per yarn vs. strain curves under unequal biaxial tension at a strain ratio, *k* =  $\varepsilon_{\text{weft}}/\varepsilon_{\text{warp}}$  = 2.

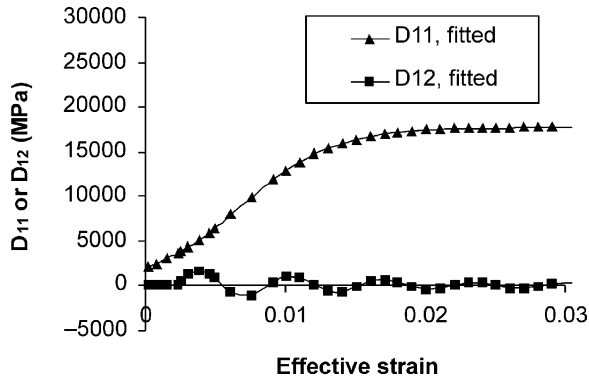


Fig. 6. Tensile properties of balanced plain weave glass fabric.

data, as shown in Fig. 5(b), the obtained equivalent tensile properties are

$$D_{11} = \frac{16000}{0.9 + 7 e^{-300\varepsilon^+}} \quad (\text{MPa}) \quad (20)$$

$$D_{12} = 2200 e^{-73\varepsilon^+} \sin(960\varepsilon^+ + 4.1) + 70 \quad (\text{MPa}) \quad (21)$$

$$D_{22} = D_{11}$$

$$D_{21} = D_{12}$$

The non-linear functions,  $D_{11}$  and  $D_{12}$ , vary with the effective strain  $\varepsilon^+$ , as shown in Fig. 6. The value of  $D_{12}$  is much smaller compared with that of  $D_{11}$ .

### 3.4.2. Determination of the shear property

The trellising shear frame used in the experiments [19] is shown in Fig. 7. The shear fixture was made of aluminum material. The woven composite patch of a size  $240 \times 240 \text{ mm}^2$  was clamped onto the frame by means of toggle clamps and a grooved surface to prevent the material from slipping. The shear angle is defined as the angle change from a right angle after shear deformation. Thus, the shear angle starting at  $0^\circ$  increases as the trellising frame deforms and it can be expressed as

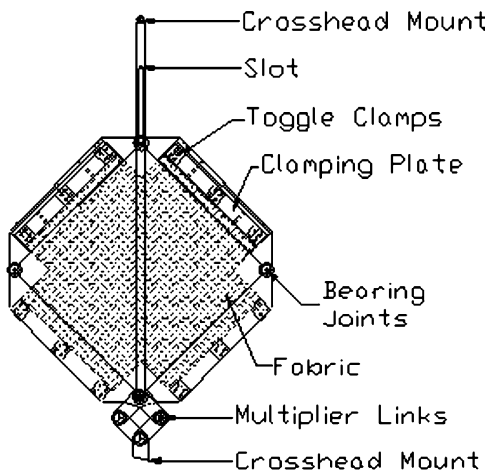


Fig. 7. Shear frame for the trellising test [19].

$$\gamma = \frac{\pi}{2} - 2 \cos^{-1} \left( \frac{u}{2a} + \frac{\sqrt{2}}{2} \right) \quad (22)$$

where  $u$  is the end nodal displacement along the  $x$  direction and  $a$  is the width of the square composite patch. A typical curve of load vs. shear angle is given in Fig. 8.

In order to determine the shear property of the material, a woven composite patch with the same size as the tested sample and with the warp and weft yarns parallel to the edges of the patch, is discretized by  $10 \times 10$  identical shell elements (element type S4R in ABAQUS). Boundary conditions are prescribed to reflect the behavior of the experimental trellising shear frame, that is, the four edges of the composite patch can only rotate rigidly around the corner points, respectively. An increasing displacement is imposed along the diagonal direction of the patch. The reaction force and the end nodal displacement are recorded. By fitting the load vs. shear deformation curve to the experimental data, as shown in Fig. 8,  $D_{33}$  can be determined as

$$D_{33} = \begin{cases} 3.08\gamma & \gamma < 0.3 \\ -15.21\gamma^4 + 36.95\gamma^3 - 12.65\gamma^2 + 3.3\gamma & \gamma \geq 0.3 \end{cases} \quad (\text{MPa}) \quad (23)$$

From Fig. 9 it can be seen clearly that the woven composite has a much smaller in-plane shear stiffness compared to tensile stiffness. This leads to the large angle variations between the warp and weft directions in forming. The square net architecture exhibits a great deformation potential with a low applied load.

Fig. 8 indicates that the force along the bias direction increases nonlinearly with the displacement. The curve consists of two parts. The first flat part at low loads is due to the trellising effect. In the second part, the load increases rapidly with the increase of the displacement, which corresponds to the shear properties of the woven composites beyond the locking angle. Once the locking angle is

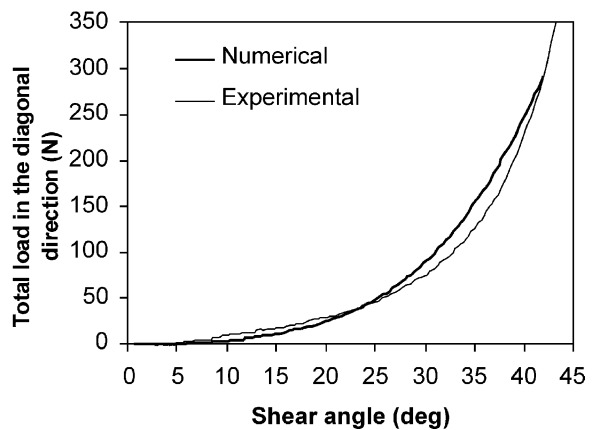


Fig. 8. Experimental data [19] and the fitting curve for the trellising shear frame test.

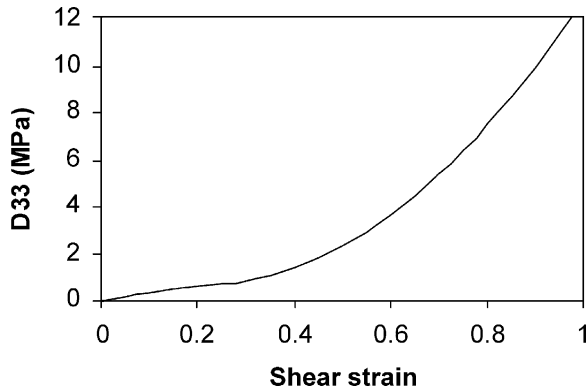


Fig. 9. Shear property of the glass/PP woven composite.

reached, the yarns interfere with each other and start to wrinkle out of the plane.

4. Validation of the material model

The constitutive model proposed in this paper can be used to efficiently predict material responses under various loading paths for woven composites with different weave architectures. In order to validate the proposed model, uniaxial tension, biaxial tension and a trellising shear frame with composites misaligned are simulated and compared with the experimental results in this section.

4.1. Case 1. Uniaxial tension and biaxial tension

In the two cases, the material under consideration is that used in Ref. [14] and Section 3.4.1. The equivalent tensile properties are obtained from an unequal biaxial tension test and are described in Eqs. (20) and (21). Here, finite element simulations of this material subjected to uniaxial tension and equal biaxial extension are conducted. The resulting load per yarn vs. tensile strain  $\epsilon_x$  curves are presented in Fig. 10. Comparing with the experimental results for equal biaxial tension  $k = 1$  and the uniaxial tension [14], it is obvious that the numerical predictions agree very well with the experimental results.

From these curves it can be concluded that the behavior of the woven fabric is non-linear at the initial stage, which is the consequence of undulation. The nonlinear zone depends on the imposed strain ratio. The property is clearly biaxial, that is, the behavior in one direction is affected by the characteristic parameters in the other direction. After the initial nonlinear range, the material behaves almost linearly, which is similar to that of the yarn alone.

4.2. Case 2. Trellising shear frame with composites misaligned

Despite similar test conditions and materials used in the experiments, variations in the results, sometimes significant,

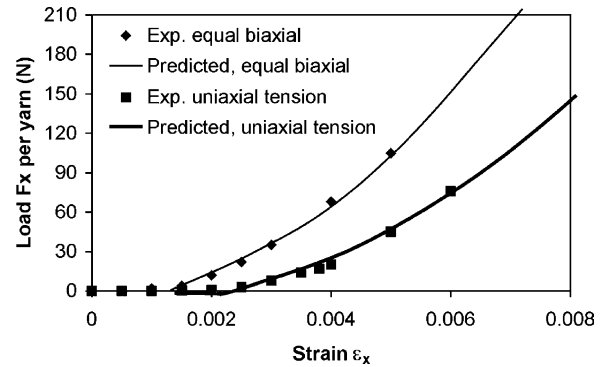


Fig. 10. Comparison of load per yarn vs. tensile strain curves under uniaxial tension and equal biaxial tension. The experimental results are from Ref. [14].

were found in the literature. In order to understand the behavior of the material, the composite was purposely misaligned in Ref. [15]. Here, the trellising shear frame with misalignment is simulated numerically and compared with the experimental results.

In this case, the yarns of the woven fabric are not parallel to the edges of the composite patch. A variable  $\varphi$  shown in Fig. 11(a) depicts the angle between the warp direction and the edge of the patch, called the off-angle. Notice that the off-angle varies in the shear frame test with the increase of the shear strain. It satisfies the following equation during deformation, that is

$$\varphi = \varphi_0(1 - 2\gamma/\pi) \tag{24}$$

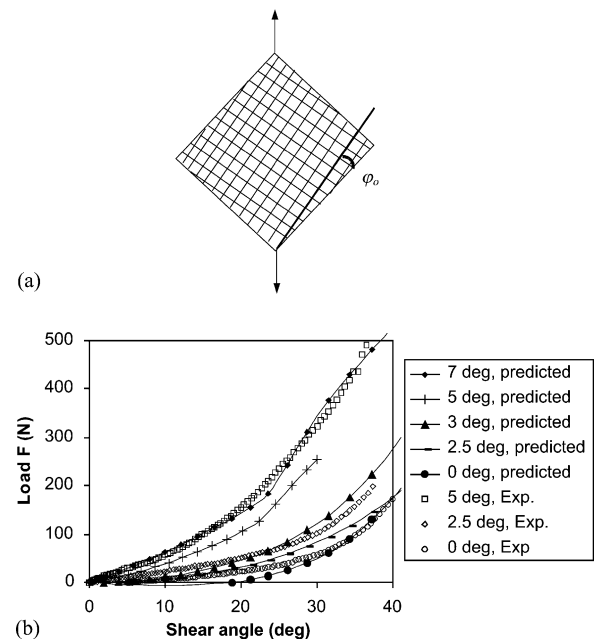


Fig. 11. Trellising shear frame test with misaligned sheets. (a) Schematic of the set-up with an initial off-angle  $\varphi_0$ ; (b) comparison of load vs. displacement curves between our predictions and the experimental results in Ref. [15].

where  $\varphi_0$  is the initial off-angle,  $\varphi$  and  $\gamma$  are the current off-angle and shear strain, respectively. The composite patches with off-angles  $\varphi_0$  of 0, 2.5, 3, 5 and 7° are simulated.

In Section 3.4.2, the shear property,  $D_{33}$ , was obtained by fitting the average of several 0° off-angle shear tests. Unfortunately, the experimental data of tensile tests of this material are not available in the literature. Therefore, numerical biaxial tests were performed to obtain  $D_{11}$  and  $D_{12}$ . As presented in our previous work [21], the woven architecture can be modeled by a unit cell in the FEM analysis. Numerical tests on the unit cell can provide the necessary load vs. displacement curves in determining  $D_{11}$  and  $D_{12}$ . For the balanced plain weave glass fabric reinforced composite used in Ref. [15],  $D_{11}$  and  $D_{12}$  were obtained as

$$D_{11} = \frac{12\,600}{1 + e^{-280\varepsilon^+}} \quad (\text{MPa}) \quad (25)$$

$$D_{12} = 1100 e^{-73\varepsilon^+} \sin(80\varepsilon^+ - 6.1) + 50 \quad (\text{MPa}) \quad (26)$$

The shear property is given in Eq. (23).

The off-angle  $\varphi$  can be reflected in the constitutive equation (9) by an additional transformation matrix.  $\varphi$  is negative if the rotation from the warp direction to the  $X$  is clockwise and positive if counter-clockwise. The resulting force–displacement curves are obtained, as shown in Fig. 11(b). The case of trellising shear frame with composites misaligned involves a combination of shear and tension. It is found that with the increase of the off-angle, the pulling force increases rapidly as the tensile deformation becomes dominant earlier in the deformation. Compared with experimental data [15], the predictions by our model are very reasonable. The numerical simulations for 3 and 7° cases match almost perfectly with the experimental data in 2.5 and 5° cases, respectively. The errors may come from the assumptions made in numerical simulations, for example, no-slip boundary conditions under clamps, and the angle measurement in experiments considering the sensitivity of the material to the off-angles.

## 5. Discussion and future work

The comparison of the numerical simulations with the experimental data published in the literature [14,15] is very encouraging, as shown in Section 4. Here, we discuss various aspects of this new constitutive model to provide a comprehensive understanding of this model.

### 5.1. Significance of the non-orthogonal transformation matrices

A non-orthogonal constitutive model is necessary, especially when composites experience large deformation. Take the trellising shear frame test in Section 3.4.2, for example. Here, two cases are simulated, one uses our

non-orthogonal material model and the other uses the conventional material model, which considered only the orthogonal transformation, i.e. in this case, matrices  $T_2$  and  $T_3$  in the form of Eqs. (11) and (12). Comparing the load vs. displacement curves obtained by the two approaches, as given in Fig. 12, it is obvious that the ignorance of the non-orthogonal nature of the woven fabric in large deformation will result in a much higher force prediction and unreasonable results, i.e.  $F_x \neq F_y$  in the trellising shear frame test case, which is supposed to be the same since the material and boundary conditions are inter-changeable. Similarly, in the off-angle tests, when  $T_2$  and  $T_3$  were not considered, the predicted forces were about six times the actual ones. This could lead to a convergence problem in the FEM simulations.

### 5.2. Architectures of woven fabric

Woven fabrics possess similar deformation mechanisms in nature and fabric structures can be repeated by an elementary pattern. Therefore, for the woven composites with different architecture reinforcement, the proposed non-orthogonal constitutive model and its implementation procedure can be applied to predict the nonlinear material properties and the response under various loading paths.

Take the 2 × 2 twill woven fabric, shown in Fig. 1(c), as an example. The density and crimp of the fabric are 0.35 (yarn/mm) and 0.35%, respectively. The equivalent properties in our material models can be obtained following a similar procedure as illustrated in Section 3.4. Thus, the response of the material under various loading paths can be predicted. Fig. 13 presents the experimental [14] and numerical results using our model for the 2 × 2 twill carbon fabric under biaxial tension at various strain ratios. It can be seen that the predictions given by our model agree very well with the experimental data.

For unbalanced fabric reinforced composites, different  $D_{11}$  and  $D_{22}$  values and potentially different  $D_{12}$  and  $D_{21}$  values are allowed in the developed material model, although some numerical problems may run into if the  $D$  matrix is not positive definite. To account for the different

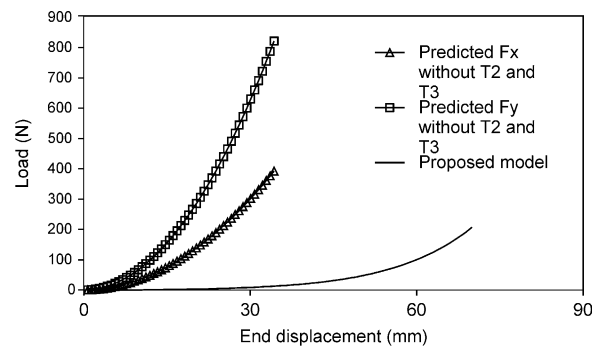


Fig. 12. Comparison of load vs. displacement curves obtained from our non-orthogonal material model and from that with only orthogonal transformations.

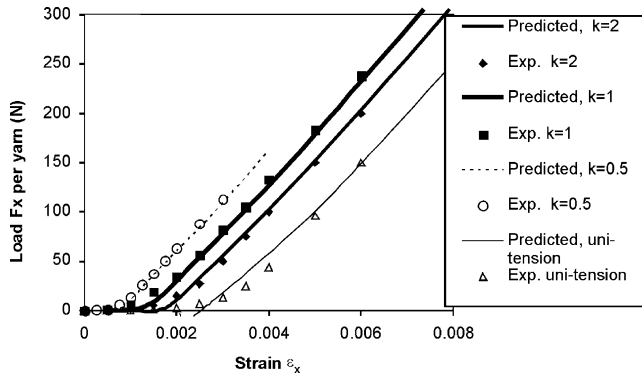


Fig. 13. Load per yarn vs. strain curves of  $2 \times 2$  twill carbon fabric under biaxial tension at various strain ratios.

shear resistance in both directions,  $\beta$  in Eq. (5) can be adjusted to reflect the difference. For the balanced structure examined in this paper,  $\beta$  is set to be 1.

### 5.3. Effect of the cross-stiffness term $D_{12}$

The response of the woven composites under different loading paths depends not only on the architecture of the woven fabric, but also on the material properties. The element  $D_{11}$  in the constitutive equation mainly associates with the tensile property along the loading direction, and the element  $D_{12}$  reflects the compaction as well as the effect of the property along the other direction on that in the loading direction.

For the plain woven composite examined in this paper,  $D_{12}$  is much smaller than  $D_{11}$ , especially at large strains. This is due to a small shrinkage of the fabric in the transverse direction when it is subjected to tension along its longitudinal direction. From the observation of the fitted  $D_{12}$  in Fig. 6, it is reasonable to assume  $D_{12}$  as a constant. Fig. 14 examines the effects of  $D_{12}$  on the load vs. strain response for the balanced plain weave glass fabric under unequal biaxial tension, where the imposed displacement in the  $x$  direction is twice that in the  $y$  direction. Three different values are examined to study the effect of  $D_{12}$  on the overall material response. They are  $D_{12}$  follows Eq. (21), takes the maximum value of the function, 1728 MPa, and the average value, 187 MPa. It appears that  $D_{12}$  affects the response along the  $y$  direction more than that in the  $x$  direction when the strain ratio is 0.5. Also, it is found that when  $D_{12}$  is taken to be a constant at the average value, the result is still acceptable. Therefore, to simplify the analysis and to avoid any convergence problem in FEM simulations associated with a negative stiffness number,  $D_{12}$  can be taken as a positive constant in simulating a forming process of balanced plain weave composite.

### 5.4. Temperature effect

During thermo-stamping, the matrix material in the commingled woven fabric becomes melted at high

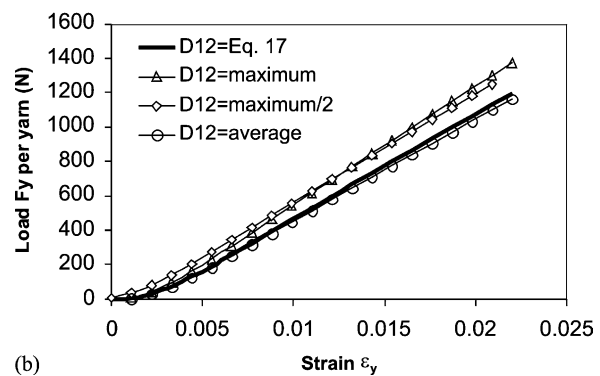
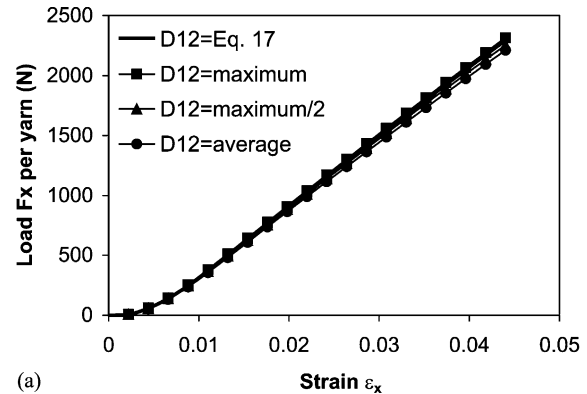


Fig. 14. Effects of  $D_{12}$  on the load per yarn vs. strain response for the balanced plain weave fabric under unequal biaxial tension (a) along the  $x$  direction; (b) along the  $y$  direction.

temperatures. At the melting temperature, the resin provides little resistance to shear. The viscosity of the resin and the processing conditions need to be involved in this model, which relates stress to strain rate and temperature. This work is currently under investigation.

## 6. Conclusions

On the basis of stress and strain analysis in both the orthogonal and non-orthogonal coordinates, as well as the rigid body rotation matrices, a non-orthogonal constitutive model and its numerical implementation procedure for woven composite under large deformation is developed in this paper. Basic assumptions used in this model include (1) incompressibility; (2) the tensile and shear responses in the non-orthogonal material coordinates are decoupled, which was verified experimentally in Ref. [14]; and (3) negligible compressive stiffness.

The material model was implemented in a commercially available finite element package (ABAQUS/Standard) and was validated by several cases, i.e. the biaxial tension and the trellising shear frame test with the composite sheets misaligned by an off-angle. The predictions by the proposed model agree very well with the experimental data provided in the literatures [14,15]. This model has the advantages of being

- efficient, convenient and suitable for woven composites and woven fabric with various woven architectures;
- capable of accurately capturing material response under different loading paths;
- truthful in reflecting the complex redistribution and reorientation of fibers in the composite, i.e. non-orthogonality;
- able to account for material non-linearity and geometrical non-linearity, i.e. large displacement and finite rotation of the fibers.

It has been concluded that the non-orthogonal transformation matrices are necessary and important to accurately predict the material properties and various responses for the woven composites, especially when materials experience large deformation. Ignorance of the non-orthogonal nature of the woven fabric results in a much higher force prediction and unreasonable results (unbalanced forces for a balanced material under symmetric loading). The effect of  $D_{12}$  on fabric tensile response is much smaller than that of  $D_{11}$ . When the yarn possesses linear tensile behavior,  $D_{12}$  can be treated as a constant.

The model developed here can be used to efficiently and accurately simulate the forming of composite sheets. Further developments will include the effects of temperature and viscous behavior of the resin.

### Acknowledgments

The financial supports from the National Science Foundation (Grant No. DMI-9900185) and Ford Motor Company are greatly appreciated. The authors would also like to thank Professor Boisse, Laboratoire de Mécanique des Systèmes et des Procédés, France, and Professor Chen, University of Massachusetts-Lowell, for sharing with us their experimental results. In addition, Professor Yu, Hong Kong University of Science and Technology, is gratefully acknowledged for valuable discussions.

### References

- [1] Van West BP, Pipes RB, Keefe M. A simulation of the draping of bi-directional fabrics over arbitrary surfaces. *J Textile Inst* 1990;81(4): 448–60.
- [2] Chou TW, Ko FK. Textile structural composite. *Composite material series*, vol. 3. Amsterdam: Elsevier; 1991.
- [3] Laroche D, Vu-Khanh T. Modelling of the forming of complex parts from fabric composites. In: Hoa SV, editor. *Development and design with advanced materials*. Amsterdam: Elsevier; 1992. p. 255–62.
- [4] Long AC, Robitaille F, Souter BJ. Mechanical modeling of in-plane shear and draping for woven and non-crimp reinforcements. *J Thermoplast Compos Mater* 2001;14(4):316–26.
- [5] Hsiao SW, Kikuchi N. Numerical analysis and optimal design of composite thermoforming process. *Comput Meth Appl Mech Engng* 1999;177:1–34.
- [6] Realf MI, Boyce MC, Backer S. A micromechanical model of the tensile behavior of woven fabric. *Textile Res J* 1997;67(6):445–59.
- [7] Ishikawa T, Chou TW. Stiffness and strength behavior of woven fabric composites. *J Mater Sci* 1982;17:3211–20.
- [8] Holzapfel GA, Gasser TC. A viscoelastic model for fiber-reinforced composites at finite strains: continuum basis, computational aspects and applications. *Comput Meth Appl Mech Engng* 2002; in press.
- [9] Luo SY, Chou TW. Finite deformation and non-linear elastic behavior of flexible composites. *J Appl Mech* 1988;55:149–55.
- [10] Luo SY, Chou TW. Finite deformation of flexible composites. *Proc R Soc Lond* 1990;A429(June):569–86.
- [11] Blanlot R, Billoët JL. Numerical formulation of the evolution anisotropic behavior of composite fabrics in order to simulation forming processes. *Proceedings of ICCM-10*, vol. 3, Whistler, BC, Canada; 1995. p. 229–36.
- [12] Vu-Khanh T, Liu B. Prediction of fiber rearrangements and thermal expansion behavior of deformed woven-fabric laminates. *Compos Sci Technol* 1995;53(2):183–91.
- [13] Cherouat A, Billoët JL. Finite element model for the simulation of prepregged woven fabric by deep-drawing and lay-up process. *J Adv Mater* 2000;32(4):42–53.
- [14] Buet-Gautier K, Boisse P. Experimental analysis and modeling of biaxial mechanical behavior of woven composite reinforcements. *Exp Mech* 2001;41(3):260–9.
- [15] Chen J, Lussier DS, Cao J, Peng XQ. Materials characterization methods and material models for stamping of plain woven composites. *Int J Forming Process* 2002; in press.
- [16] Boisse P, Gasser A, Hivet G. Analyses of fabric tensile behavior: determination of the biaxial tension-strain surfaces and their use in forming simulations. *Compos Part A: Appl Sci Manufact* 2001;32: 1395–414.
- [17] Daniel IM. *Engineering mechanics of composite materials*. New York: Oxford University Press; 1994.
- [18] Johnson W, Mellor PB. *Engineering plasticity*. London: Van Nostrand Reinhold Co; 1973.
- [19] Lussier D, Chen J. Material characterization of woven fabrics for thermoforming of composites. *Proceedings of the American Society for Composites. Fifteenth technical Conference*, College Station, Texas, USA; 2000. p. 301–10.
- [20] Cao J, Chen J, Long A, Blanchard P. Final report of workshop on composite sheet forming. <http://www.mech.northwestern.edu/fac/cao/nsfworkshop>; 2001.
- [21] Peng XQ, Cao J. A dual homogenization and finite element approach for material characterization of textile composites. *Composites, Part B* 2002; in press.